Nanotechnology **20** (2009) 505302 (7pp) doi:10.1088/0957-4484/20/50/505302

Liquid-precursor electron-beam-induced deposition of Pt nanostructures: dose, proximity, resolution

E U Donev and J T Hastings

Department of Electrical and Computer Engineering, and Center for Nanoscale Science and Engineering (CeNSE), University of Kentucky, Lexington, KY 40506, USA

E-mail: hastings@engr.uky.edu

Received 3 October 2009, in final form 2 November 2009
Published 19 November 2009
Online at stacks.iop.org/Nano/20/505302

Abstract

While electron-beam-induced deposition (EBID) from various gaseous precursors has been known and studied for decades, EBID from bulk liquid precursors is very much in its infancy and the following is only the second report on this technique. Here we present liquid-precursor (LP-)EBID of platinum (Pt) nanostructures from a dilute aqueous solution of chloroplatinic acid (H_2PtCl_6). We investigate how the lateral size of Pt nanoparticles (NPs) varies with charge dose, and how already deposited Pt NPs are affected by the subsequent deposition of their neighbors (proximity effect). We also demonstrate LP-EBID of dense arrays of small Pt dots (60 nm pitch, 30 nm diameter) and thin Pt lines (60 nm pitch, 25 nm width), which compare favorably with the typical resolution of resist-based electron-beam lithography.

(Some figures in this article are in colour only in the electronic version)

1. Introduction

Focused electron-beam-induced deposition (EBID) is a nanoscale patterning technique that has gained considerable momentum in the last decade or so [1–3]. Until very recently, EBID has always relied on the e-beam-induced dissociation of adsorbed gaseous precursors, and the low purity of the resulting deposits has been a major factor hampering a wider application of the technique. Gas-phase EBID of platinum (Pt), for instance, typically yields deposits consisting of 25–40% Pt, with the remainder taken up by other elements in the precursors such as carbon and phosphorus [4, 5]. As first reported in [6], however, we obtained deposits with 85–95% Pt content by using a bulk liquid instead of a gas as the EBID precursor. The work reported here is only the second experimental study of liquid-precursor electron-beam-induced deposition (LP-EBID), and its objective was two-fold: to observe the effects of some of the deposition parameters on the size of the Pt deposits, but also to demonstrate the potential of LP-EBID for fabricating very small and dense nanostructures. We discovered that deposition begins abruptly at a certain dose and is followed by gradual particle growth. Moreover, the relative proximity of nanostructures only mildly influences their lateral dimensions. Finally, we were able to achieve sub-30 nm dense structures with our current experimental configuration.

2. Experimental details

We deposited various Pt nanostructures from chloroplatinic acid (1% by weight H_2PtCl_6, Sigma-Aldrich Inc.) in deionized water (18 MΩ). Depositions were carried out with an electron-beam lithography tool (Raith e_LiNE), using commercial capsules (QuantomiX QX-102 WETSEM) designed to separate 15 μl of liquid from the vacuum chamber via a 150 nm thick polyimide membrane [7]. The primary e-beam energy was 20 keV; a beam current of 160 pA was used for all Pt deposits other than the parallel lines in figure 5(a), which were written at 340 pA. Colloidal gold nanoparticles, drop-cast on the side of the membrane that would be in contact with the liquid precursor, served as focusing artifacts. Deposition of Pt nanostructures begins by focusing the electron beam at the membrane–liquid interface, as depicted in figure 1, whereas the size and shape of the deposits can be varied by controlling the dwell time and scan pattern of the electron beam. In the next three sections, we quantify the effects

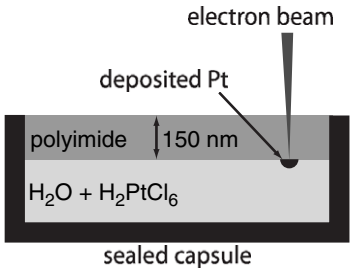

Figure 1. Schematic of liquid-precursor electron-beam-induced deposition (LP-EBID) of platinum (Pt) from aqueous solution of chloroplatinic acid ($H_2O + H_2PtCl_6$). The solution (15 μl) is separated from the vacuum chamber by a polyimide membrane and the focused electron beam deposits Pt nanostructures at the membrane–solution interface.

of dwell time (i.e. e-beam dose) and deposition sequence (i.e. proximity of deposits to one another) during LP-EBID of Pt, as well as demonstrate a practical limit to the resolution of this technique under the given deposition conditions.

3. Dose dependence

Figure 2 summarizes how the average size of Pt NPs deposited by exposing single spots in LP-EBID depends on the nominal amount of charge per particle delivered by the electron beam. Also shown are scanning electron micrographs (SEMs) of two representative graded-dose arrays of Pt NPs, where the nearest-neighbor spacings are 350 nm and the NPs along each horizontal row have nominally identical deposition doses. The two arrays cover the same dose range of 10–110 pC, bottom to top row, but differ in the sequence of deposition within the array, as indicated by the vertical arrows: bottom row deposited first ('low-dose-first') in figure 2(a) and top row deposited first ('high-dose-first') in figure 2(c). Thus, two sets of NPs with opposite deposition sequences were deposited at each investigated dose, in order to assess how the relative proximity of other NPs affects the deposition of an individual NP within an array. Section 4 explores the issue of proximity in more detail.

Lateral particle sizes were determined by image analysis of each set of SEM images using a commercial software package (IGOR Pro 6.10) and compiled as the average number of image pixels occupied by a Pt NP deposited at a given e-beam dose and deposition sequence. The size of an image pixel in nm^2 was given by the SEM system. The dose dependence for all low-dose-first Pt NPs is shown in figure 2(b), whereas part (d) refers to the high-dose-first Pt NPs. The SEM images were taken *in situ* (i.e. through the membrane) immediately after patterning and at identical magnifications. No deposition was observed at the electron doses used for imaging.

Figures 2(b) and (d) both indicate that the LP-EBID of Pt begins only after a minimum amount of electron charge has been delivered into the bulk liquid precursor. A threshold dose of 5 pC per NP, independent of deposition sequence, can be identified from the zoomed-in dose regions in the upper panels of figures 2(b) and (d), followed by a steep increase in NP size with dose up to about 12 pC per NP. Increasing the dose further continued to yield larger Pt NPs, but the growth was much more gradual relative to the initial stage, as evidenced in the lower panels of figures 2(b) and (d) by the slope of either curve between 12 and 120 pC. In fact, such two-stage mode of lateral growth—rapid increase in size followed by saturation—is consistently observed in EBID from gaseous precursors [3]. It is likely that all of our deposits also grew coaxially with the electron beam and took increasingly columnar shapes for higher doses [8, 3].

Above 120 pC, however, a subtle difference between the two curves emerges, namely that the low-dose-first Pt NPs actually shrank in lateral size (figure 2(b)), while their high-dose-first counterparts (figure 2(d)) continued to grow. For example, comparing deposits at 135 versus 165 pC per NP, the average particle areas were, respectively: (i) 7265 ± 480 versus 5815 ± 575 nm^2 when the low dose was written first (figure 2(b)); and (ii) 6730 ± 495 versus 8660 ± 705 nm^2 when the high dose was written first (figure 2(d)). We attribute this difference to a proximity effect, which we explore further in section 4, but also point out that it had a negligible effect on the deposition at low doses, including the threshold dose, as can be seen by comparing the upper panels of figures 2(b) and (d).

4. Proximity effects

A type of proximity effect sometimes observed in gas-phase EBID comes about when previously deposited structures accrue extra material due to the spraying of secondary and/or forward-scattered electrons from another structure that is currently being fabricated in their vicinity [3]. In other words, because the top row of Pt NPs in figure 2(c) was the first to be deposited in that particular array, its NPs must have experienced parasitic sidewall depositions during the fabrication of the remaining ten rows, with each subsequent row having a progressively diminishing impact on the top row because of increasing distance as well as decreasing dose. Similar reasoning can then explain why, in the low-dose-first set of NPs (figure 2(b), lower panel), the highest-dose NPs do *not* have the largest average area: the top row containing the highest-dose (165 pC) NPs was written last in its array, so that those NPs were not 'sprayed' with electrons during the fabrication of the other ten rows of the same array. On the other hand, the NPs with the third-highest dose (135 pC) accrued enough extra Pt from the depositions of the top two rows to attain the largest lateral sizes.

Figures 3(a) and (c) show SEM images of two LP-EBID structures that were deliberately meant to produce a proximity effect and better elucidate the role of deposition sequence. Each structure consisted of a single 25 pC Pt NP at the center surrounded by ten concentric rings of Pt NPs, and was deposited sequentially as indicated by the horizontal arrows: either starting with the center NP and finishing with the outermost ring ('center-NP-first'; figure 3(a)) or vice versa ('outer-ring-first'; figure 3(c)). The rings were written as lines of zero width, 150 nm nominal spacings between nearest-neighbor NPs and rings, and a dose of 25 pC per NP. Analysis of each SEM image yielded all particle areas and radial distances for the given deposition sequence, which were then sorted and averaged according to which ring the NPs belonged

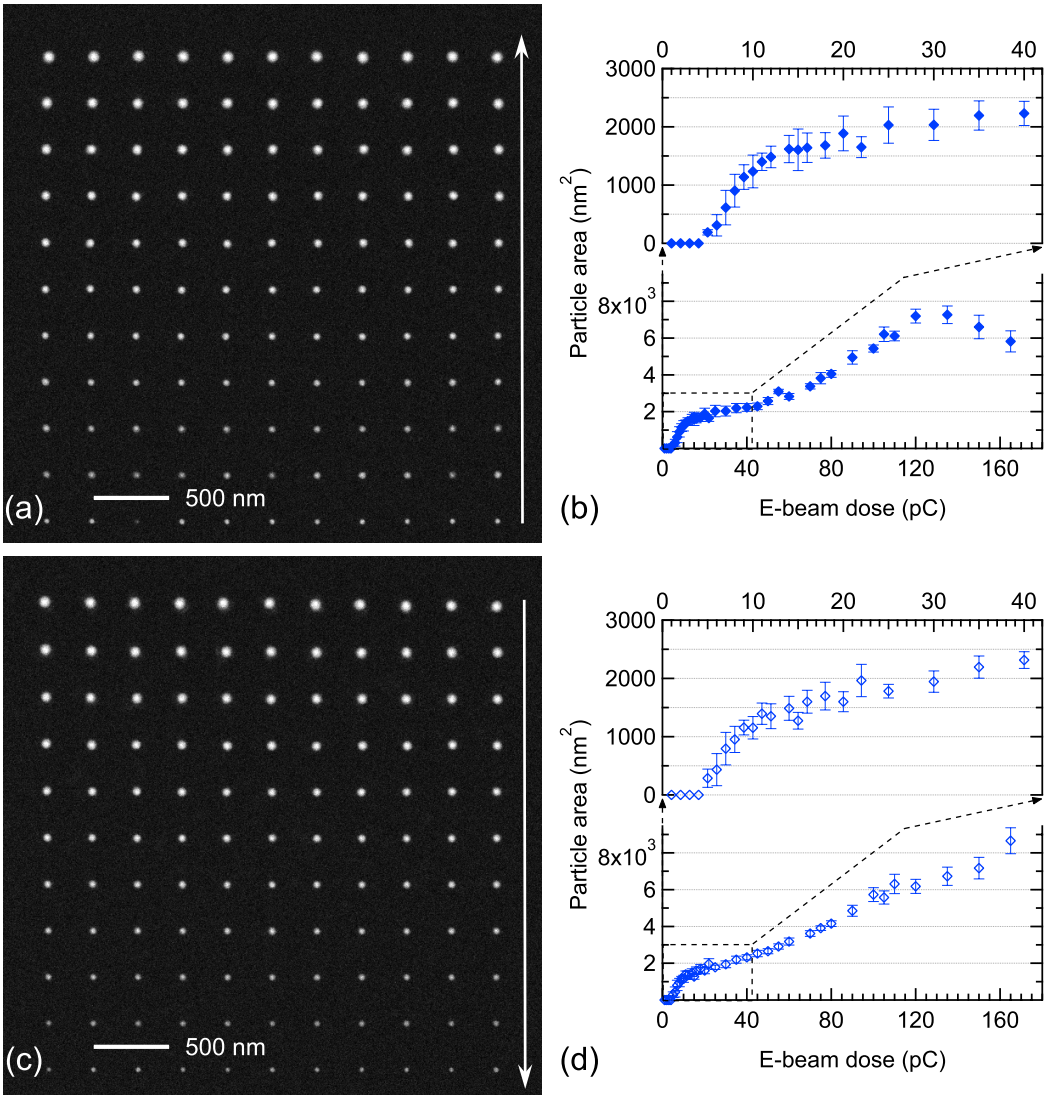

Figure 2. (a) SEM image of one of the 'low-dose-first' arrays (350 nm pitch), with Pt NPs deposited at different e-beam doses; NPs along a horizontal row have nominally equal doses, increasing by 10 pC with each row from bottom (10 pC per NP) to top (110 pC per NP); upward arrow indicates deposition sequence: bottom row (hence, 'low-dose-first') to top row. (b) Lateral area for low-dose-first Pt NPs, averaged over all same-dose NPs of the set and plotted as a function of dose for all (lower panel) or a subrange (upper panel) of the investigated doses. (c) SEM image of one of the 'high-dose-first' arrays (350 nm pitch), with Pt NPs deposited at different e-beam doses; NPs along a horizontal row have nominally equal doses, decreasing by 10 pC with each row from top (110 pC per NP) to bottom (10 pC per NP); downward arrow indicates deposition sequence: top row (hence, 'high-dose-first') to bottom row. (d) Lateral area for high-dose-first Pt NPs, averaged over all same-dose NPs of the set and plotted as a function of dose for all (lower panel) or a subrange (upper panel) of the investigated doses. All error bars represent statistical uncertainties of $\pm 1\sigma$.

to. Finally, the average lateral size of the NPs in each ring, together with the lateral size of the center NP, was plotted as a function of the average radial distance of those NPs from the center of the structure; figure 3(b) refers to the center-NP-first structure and figure 3(d) to the outer-ring-first structure.

For the center-NP-first structure (figure 3(a)), the downward trend exhibited by the lateral particle size with increasing radial distance (figure 3(b)) is largely to be expected in the presence of proximity effects, since NPs located closer to the center were fabricated earlier in the deposition sequence and thus able to gain additional material from the subsequent depositions of the remoter NPs. It is unclear, however, why the center NP remained relatively small, despite being the very first one to be deposited. Possible reasons include the larger actual radius of the innermost ring (~200 instead of 150 nm), which could have mitigated the proximity effect of the NPs in that ring on the center NP, and also the 'shadowing' [3] by NPs in the inner ring(s) of some of the high-energy, forward-scattered electrons coming from the fabrication of NPs in the outer rings, which too could have reduced the parasitic deposition of Pt on the center NP. And while shadowing would not have prevented the nine NPs in the innermost ring from spraying electrons towards the center NP, it appears that, at 25 pC per NP, the cumulative parasitic dose from those nine (and any other) NPs was insufficient to appreciably enlarge the center NP.

As for the outer-ring-first structure (figure 3(c)), a slight jump in particle size appears around 1200 nm (figure 3(d)), presumably due to parasitic depositions from the smaller

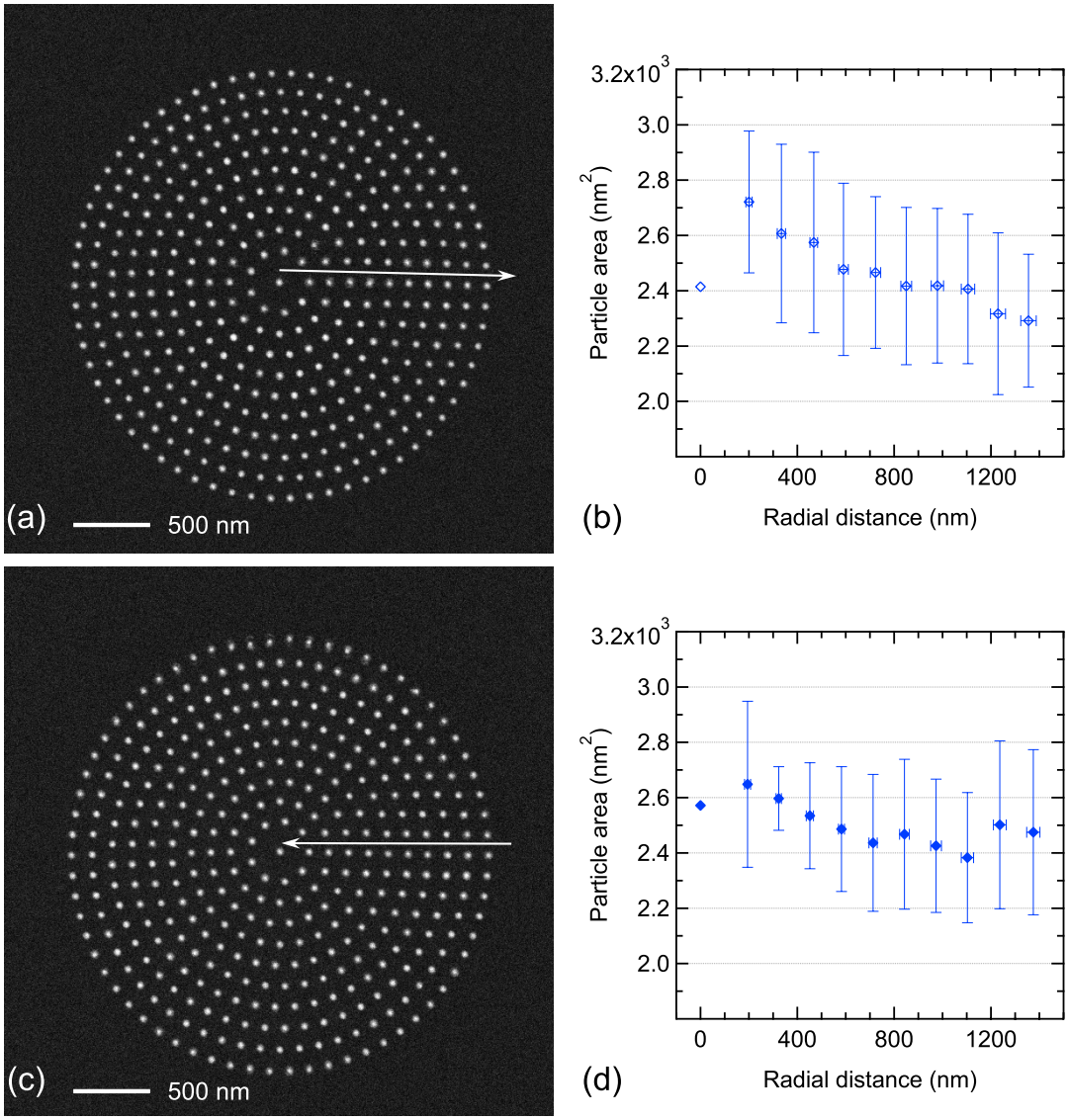

Figure 3. (a) SEM image of 'center-NP-first' structure, consisting of concentric rings of Pt NPs surrounding a single Pt NP, with intra- and inter-ring spacings of 150 nm and nominal dose of 25 pC per NP; rightward arrow indicates deposition sequence: center NP first, then ring-by-ring towards outermost ring. (b) Lateral area for center-NP-first Pt NPs, averaged within each ring and plotted as a function of average radius of the corresponding ring. (c) SEM image of 'outer-ring-first' structure, consisting of concentric rings of Pt NPs surrounding a single Pt NP, with intra- and inter-ring spacings of 150 nm and nominal dose of 25 pC per NP; leftward arrow indicates deposition sequence: outermost ring first, then ring-by-ring towards center NP. (d) Lateral area for outer-ring-first Pt NPs, averaged within each ring and plotted as a function of average radius of the corresponding ring. All error bars represent statistical uncertainties of $\pm 1\sigma$.

subsequent rings, rendering the NPs in the two outermost rings of this structure somewhat larger than their counterparts in the center-NP-first structure. Contrary to expectations, however, the innermost ring again yielded the largest NPs, while the center NP, despite being last in this deposition sequence, turned out larger than its center-NP-first counterpart.

Overall, we learned that even at a relatively small particle spacing (150 nm) and high electron dose (25 pC) the proximity effects in LP-EBID of Pt are weak but not indiscernible.

5. Resolution

We present in this section two exemplar nanostructures that demonstrate the ability of the LP-EBID technique to fabricate densely packed arrays of very small features: lines and dots of 25–30 nm width or diameter at a pitch of 60 nm. Such feature sizes and spacings are a factor of ∼5 larger than the resolution limits of resist-based electron-beam lithography (EBL); for example, see [9, 10]. Unlike EBL, however, LP-EBID is a direct-write technique, in the sense that fabrication of metal nanostructures is typically accomplished in a single step, without additional chemical or physical post-processing of the patterned areas.

Figure 4(a) shows an SEM image of a square array of Pt dots, which was deposited in area exposure mode with a nominal step size of 60 nm and dose of 8 pC per step (NP). Analysis of the SEM image data yielded the lateral size distribution in figure 4(b), where 80% of the dots have effective diameters between 20 and 30 nm. Since the array

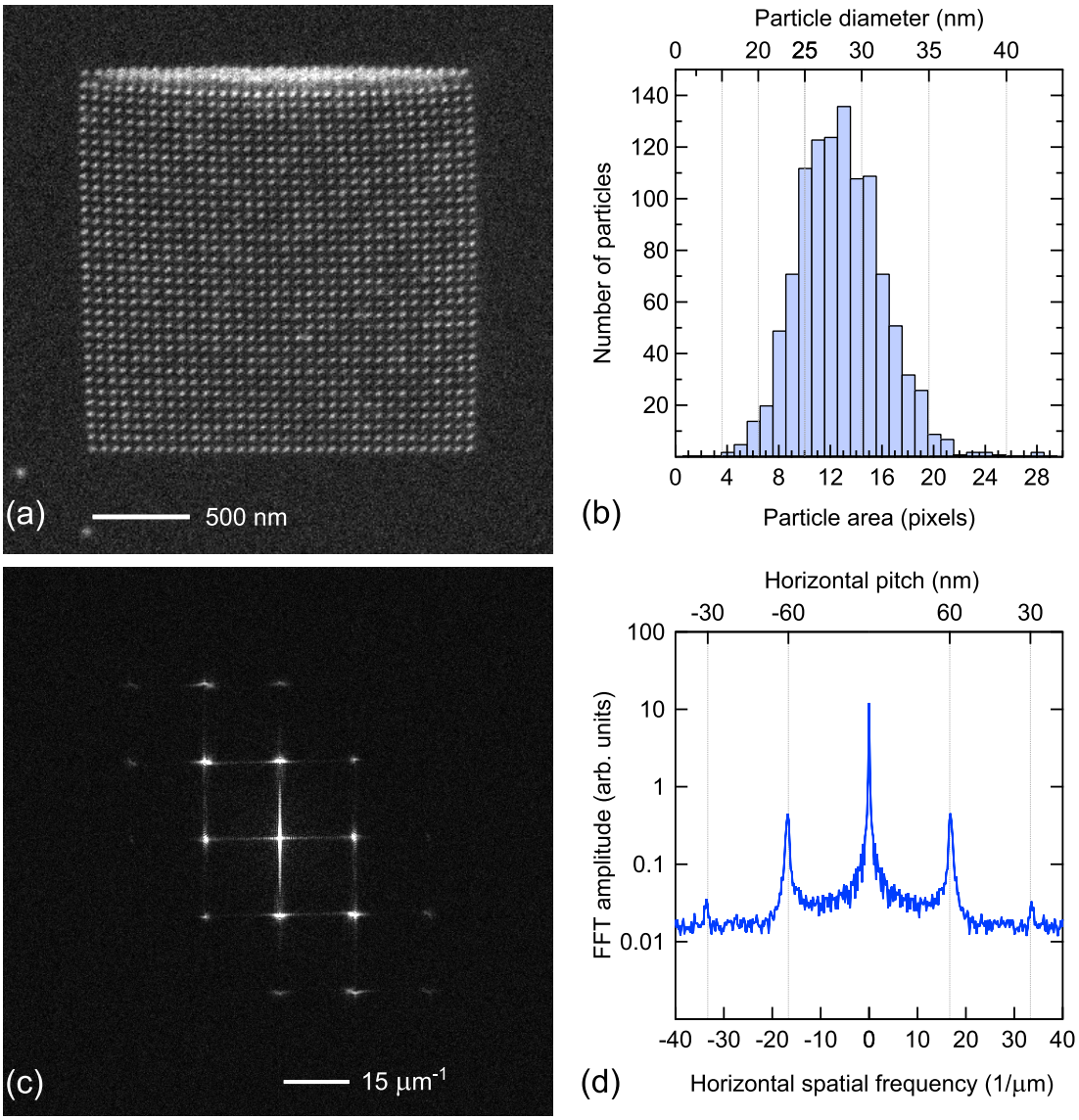

Figure 4. (a) SEM image of dense array of small Pt NPs (dots) deposited by LP-EBID. (b) Lateral size distribution of Pt dots in (a), plotted in terms of number of image pixels occupied by a dot and effective diameter (assuming dots with circular cross-sections); 80% of all dots have diameters between 20 and 30 nm. (c) 2D-FFT image of Pt dots in (a), displaying the periodic structure of the array in reciprocal space. (d) Horizontal linear profile plotted along the bright spots in the middle of 2D-FFT image in (c); pairs of first and second Fourier harmonics confirm horizontal pitch of 60 nm for Pt dots in (a).

was written by scanning the e-beam horizontally from top to bottom, parasitic deposition due to proximity effects likely caused the first couple of rows to become smeared and distorted (figure 4(a)), and they were therefore excluded from the size analysis. In fact, depositing dots with a pitch of 50 nm resulted in a significantly distorted and disordered array (not shown), although most of the individual dots were still resolvable. The actual periodicity of the array in figure 4(a) was determined by performing a two-dimensional fast Fourier transform (2D-FFT) on the SEM image using a free software package (Gwyddion 2.16). Figure 4(c) visualizes the result of the FFT operation and (d) plots a linear profile taken horizontally across the middle of the 2D-FFT image in (c). The locations of the pairs of first- and second-order peaks in the FFT spectrum clearly confirm a horizontal pitch of 60 nm between the Pt dots.

Figure 5(a) is an SEM image of an array of parallel Pt lines, deposited in area exposure mode with a 60 nm step size and dose of 7 pC per step, but with a beam spot that was stigmated in the vertical direction. A horizontal linear profile crossing all the Pt lines in the middle of the SEM image is plotted in the lower panel of figure 5(b), while the upper panel expands the view of eight of the lines and allows an estimate of the average lateral linewidth: 25 ± 5 nm. Again, the 60 nm horizontal pitch of the array was confirmed by FFT analysis of the SEM image, the result of which is displayed in figure 5(c) and the horizontal linear profile across the middle of that 2D-FFT image is plotted in (d). Using a non-stigmated beam spot, we were able to deposit parallel Pt lines (not shown) of the same horizontal pitch (60 nm) by decreasing the vertical step size down to 30 nm and the dose to 3 pC per step; the resulting linewidths were about 20 nm.

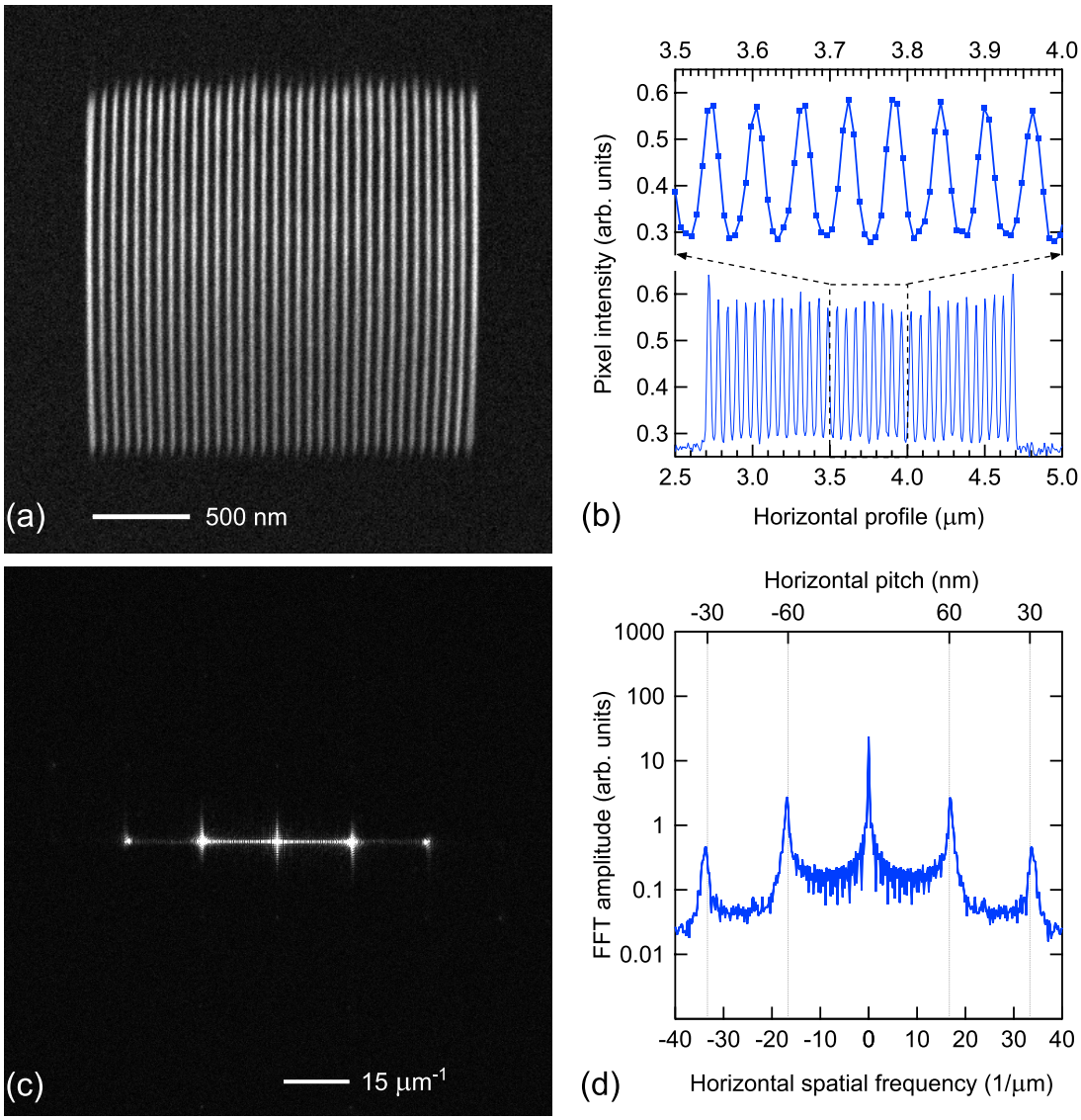

Figure 5. (a) SEM image of array of parallel Pt lines deposited by LP-EBID. (b) Horizontal linear profile, extracted from the middle of SEM image in (a) and averaged over width of 10 image pixels, spanning all (lower panel) or a subset (upper panel) of the Pt lines; 25 ± 5 nm full linewidth at half maximum of pixel intensity. (c) 2D-FFT image of Pt lines in (a), displaying the periodic structure of the array in reciprocal space. (d) Horizontal linear profile plotted along the bright spots in the middle of 2D-FFT image in (c); pairs of first and second Fourier harmonics confirm horizontal pitch of 60 nm for Pt lines in (a).

6. Conclusions

We have explored in this work three aspects of electron-beam-induced deposition of platinum nanostructures from a bulk liquid precursor (LP-EBID of Pt), namely the dose-size relationship, proximity effects, and resolution. A threshold dose of 5 pC per nanoparticle (NP) was necessary for the deposition of Pt NPs in square arrays of 350 nm periodicity. Above threshold, the lateral size of the NPs exhibited three stages of growth as a function of e-beam dose: rapid initial increase (5–12 pC); tendency towards saturation (12–120 pC); and dependency on the spatio-temporal location of a given NP within the array, i.e. proximity effects, but only at doses ∼25 times higher than the threshold dose (120–165 pC).

Furthermore, proximity effects did not seem to influence the threshold dose for LP-EBID of Pt, contrary to what generally happens in resist-based e-beam lithography. Another type of Pt nanostructure, a central NP surrounded by concentric rings of NPs spaced by 150 nm, was expected to throw more light on the issue of proximity, but the possible competition between parasitic deposition on the one hand and the blocking of forward-scattered electrons on the other resulted in the size variation due to proximity effects being similar to the inherent statistical variability between particles.

Regarding resolution, we demonstrated that LP-EBID of Pt is capable of producing 30 nm (and smaller) NPs in a square array of 60 nm pitch, as well as 25 nm wide parallel lines separated by 60 nm. The resolution is limited by pattern distortion that may stem from proximity effects and/or membrane distortion.

Several questions require further study. For example, how does the *vertical* size of Pt deposits vary with e-beam dose?

What role does the substrate (here, the polyimide membrane) play in the deposition process? How does LP-EBID of gold and other metals differ from LP-EBID of Pt? From a fundamental point of view, what interactions govern the nucleation and growth of deposits in LP-EBID, and how do they compare with the mechanisms at work in traditional gas-phase EBID? From a technical standpoint, the high purity [6], reasonably low threshold dose, minimal proximity effects, and high resolution of LP-EBID all make it a promising technique for nanoscale patterning.

Acknowledgments

This work was supported by the Kentucky Science and Engineering Foundation under Grant KSEF-148-502-08-240. The authors thank Brian Wajdyk at CeNSE for assistance with the e-beam system.

References

[1] Silvis-Cividjian N and Hagen C W 2006 *Electron-Beam-Induced Nanometer-Scale Deposition* (*Advances in Imaging and Electron Physics*) (San Diego, CA: Academic)
[2] Randolph S J, Fowlkes J D and Rack P D 2006 *Crit. Rev. Solid State Mater. Sci.* **31** 55–89
[3] van Dorp W F and Hagen C W 2008 *J. Appl. Phys.* **104** 081301
[4] Botman A, Mulders J J L, Weemaes R and Mentink S 2006 *Nanotechnology* **17** 3779–85
[5] Wang S, Sun Y-M, Wang Q and White J M 2004 *J. Vac. Sci. Technol.* B **22** 1803–6
[6] Donev E U and Hastings J T 2009 *Nano Lett.* **9** 2715–8
[7] Thiberge S, Zik O and Moses E 2004 *Rev. Sci. Instrum.* **75** 2280–9
[8] Friedli V, Utke I, Molhave K and Michler J 2009 *Nanotechnology* **20** 385304
[9] Xu W, Wong J, Cheng C C, Johnson R and Scherer A 1995 *J. Vac. Sci. Technol.* B **13** 2372–5
[10] Fischer P B and Chou S Y 1993 *Appl. Phys. Lett.* **62** 2989–91